Available online at www.sciencedirect.com
SCIENCE DIRECT®
Real-Time Imaging 10 (2004) 239–250
www.elsevier.com/locate/rti

Morphometrical data analysis using wavelets

C.M. Takemura[a,*], R.M. Cesar- Jr.[a], R.A.T. Arantes[b], L. da F. Costa[b], E. Hingst-Zaher[c], V. Bonato[d], S.F. dos Reis[e]

[a]*Departamento de Ciência da Computação, Instututo de Matemática e Estatística da Universidade de São Paulo (USP-IME), 1010 Rua do Matão, Cidade Universitária,CEP 05508-090, São Paulo, SP, Brazil*
[b]*USP-IFSC, Av. Trabalhador Sãocarlense, 400Caixa Postal 369, CEP 13560-970, São Carlos, SP, Brazil*
[c]*USP-MZUSP, Av. Nazaré, 481 Bairro do Ipiranga,CEP 04263-000, São Paulo, SP, Brazil*
[d]*CREUPI-ICB, Av. Hélio Vergueiro Leite s/n,CEP 13990-000, Espírito Santo do Pinhal, SP, Brazil*
[e]*UNICAMP-IB, Cidade Universitária "Zeferino Vaz", CEP 13083-970, Campinas, SP, Brazil*

Available online 10 August 2004

Abstract

In this paper, we present a new shape analysis approach using the well-known wavelet transform and exploring shape representation by landmarks. First, we describe the approach adopted to represent the landmarks data as parametric signals. Then, we show the relation of the derivatives of Gaussian wavelet transform applied to the signal-to-differential properties of the shape that it represents. We present experimental results using real data to show how it is possible to characterize shapes through multiscale and differential signal-processing techniques in order to relate morphological variables with phylogenetic signal, environmental factors and sexual dimorphism. The goal of this research is to develop an effective wavelet transform-based method to represent and classify multiple classes of shapes given by landmarks.

1. Introduction

The relationship between phenotype and pre-determined time–space or genetic conditions has been the focus of many works presented to the scientific community. This kind of analysis usually involves morphometry, which can be described as the study of biological shapes. Traditional morphometrics generally apply multivariate statistical methods to size or shape variables such as distances and angles [1–3]. On the other hand, geometric morphometrics deals with geometrical relationships between these measurements [4]. Note that morphometrics is a multidisciplinary area related to shape analysis [5,6]. Nevertheless, there are few works that explore well-known multiscale and differential methods in the shape analysis and image processing community, e.g. wavelets [7–9], a gap that is partially filled by the method introduced in this paper.

Many problems in a wide variety of disciplines may be addressed in terms of computer vision concepts and methods and it is possible to reduce many of these problems to shape analysis [5], where visual information like color, texture and motion can be discarded.

The wavelet transform is a particularly useful tool to analyze non-stationary signals presenting local events because of its local analysis property [10,11]. Furthermore, its scaling properties have been extensively used to implement multiscale tools for signal analysis, thus explaining its popularity in several practical applications [12,13].

The goal of the present work is to review and generalize the work presented in [6] where 2D landmark data sets were analyzed through the wavelet transform,

*Corresponding author.
E-mail addresses: maki@vision.ime.usp.br (C.M. Takemura), cesar@vision.ime.usp.br (R.M. Cesar- Jr.).
URL: http://www.ime.usp.br/~cesar/.

1077-2014/$ - see front matter © 2004 Elsevier Ltd. All rights reserved.
doi:10.1016/j.rti.2004.05.006

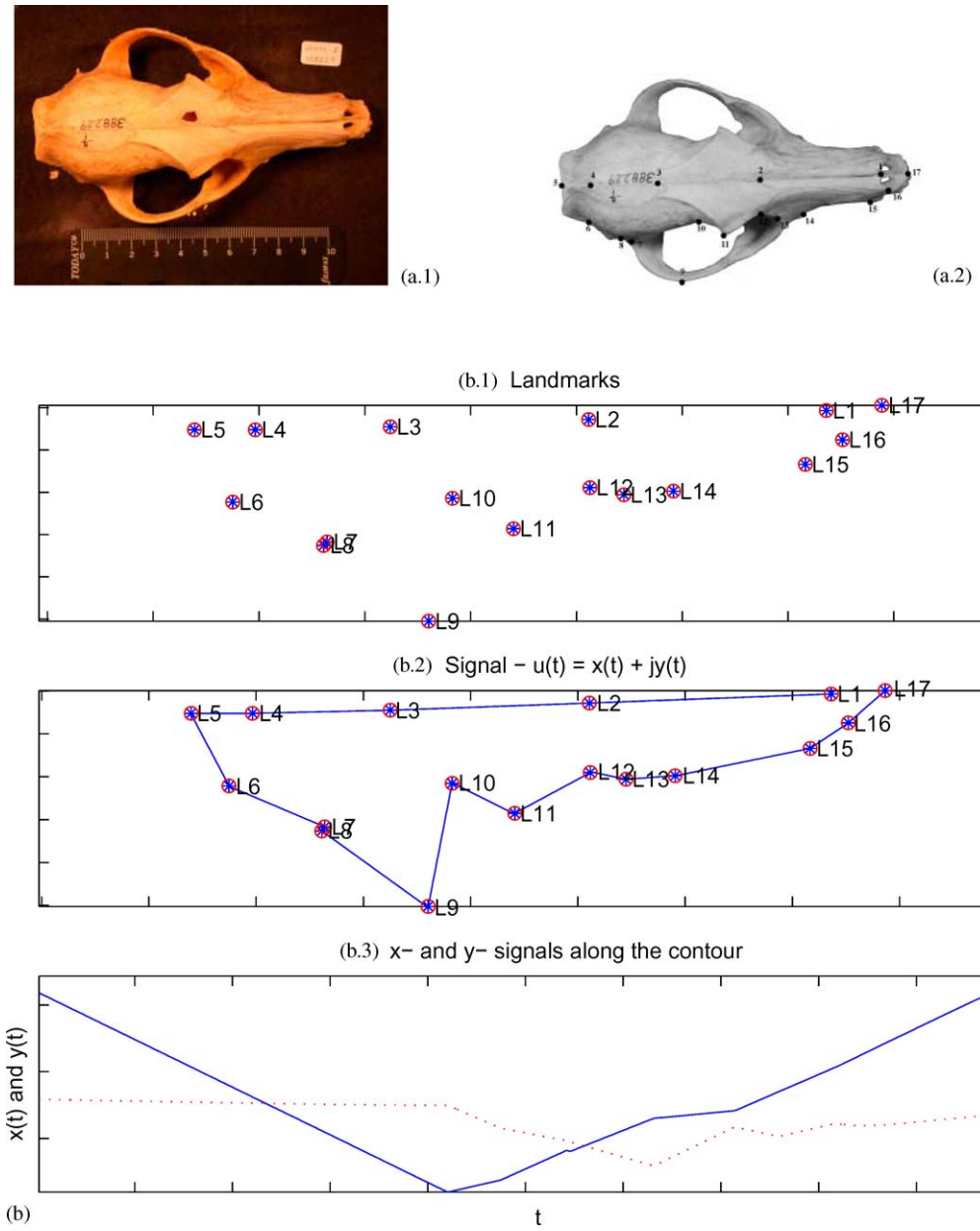

Fig. 1. (a.1) Initial image; (a.2) landmarks; (b.1) landmarks taken from (a.1); (b.2) complex-signal extracted from (b.1) and (b.3) x- and y-components of (b.2).

i.e. by formulating a signal-processing solution to 2D and 3D morphometrics. We analyze two different data sets: (a) morphological traits of 10 species of South American Canids expressed by 2D landmarks, taken from the dorsal view of the skull; (b) phenotype of specimens belonging to 5 species in a monophyletic lineage of rodents of the genus *Trinomys*, which are represented by 3D landmarks, digitized over the skull of the analyzed specimens.

In the first analysis, the intraspecific variability in biological species is the main interest while differences among males and females are also considered. Here, we examine patterns of sexual dimorphism among the sexes in a monophyletic clade formed by the South American Canids. In the family *Canidae*, broadly distributed throughout the world, differences in size and shape between sexes are usually related to mating systems and social organization. The South American members are among the less studied of the dogs, and little is known about possible differences among individuals of the same species.

As far as the 3D data is concerned, the interest is to determine whether morphological descriptors can be matched to phylogenetic trees or whether the ecological differentiation that may result from colonization of different environments. The expected result, from an

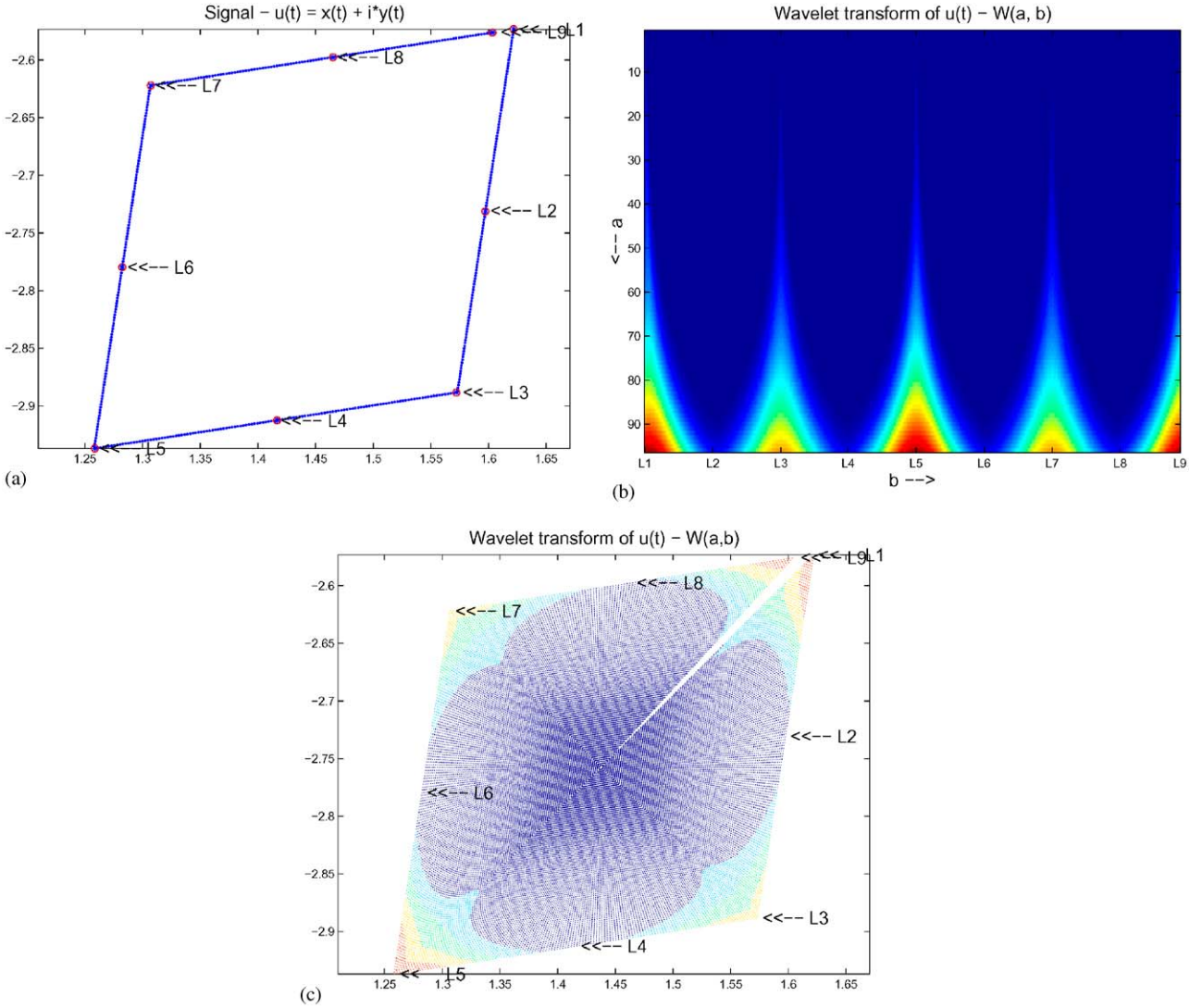

Fig. 2. (a) $u(t)$ complex signal; (b) wavelet transform with second derivative of gaussian as mother wavelet; (c) internal representation of (b): relation of (b) and the curvature of $u(t)$. The internal representation has been suggested by Prof. Pete Lestrel.

evolutionary theory viewpoint, is some inference about an evolutive trace [14] between the studied species through a comparative study concerned with relation of wavelet coefficients to shape of these species [15,16].

This work is organized as follows. In order to appreciate the use of shape analysis tools in morphometry, Section 2 describes how it is possible to extract wavelets representations of shapes described by landmarks. In the Section 3, we show a process by which it is possible to use the wavelet transform to analyze 2D and 3D signals based on a useful geometrical interpretation. Experimental results obtained using simulated and real data will be presented in Section 4. The paper is concluded with a discussion of the methodology and the successful biological results produced with the wavelet-based analysis of the real data sets.

2. From landmarks to signals

Usually landmarks represent curvature extremes or junctions between structures in key regions of the shape [17,18]. The morphometric concept of homology [1] (e.g. a landmark l in shape a corresponds to the same morphological structure that the landmark l in another shape b) allows the landmarks from all shapes to be ordered in a consistent manner (Fig. 1(b.1)). The sequence of ordered landmarks can be viewed as the vertices of a polygonal line, which can subsequently be interpolated [6] (Fig. 1(b.2)). Note that it allows the comparison between the shapes using only landmark-related values. Therefore, a landmark set L is interpolated generating a set of points denoted as $u(t) = x(t) + jy(t)$ and $\vec{u}(t) = (x(t), y(t), z(t))$ in the 2D and 3D case, respectively, to

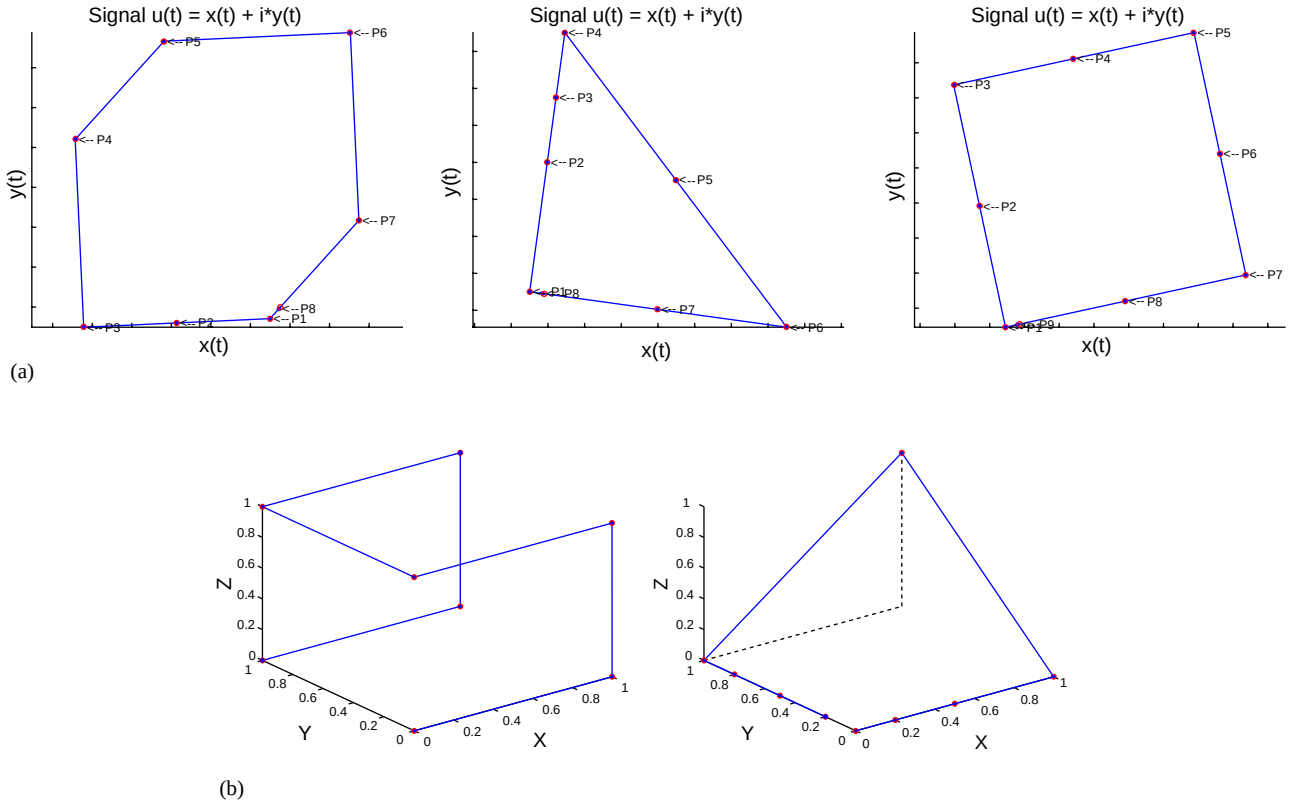

Fig. 3. (a) Models used to simulate the 2D data and (b) two of the models used to simulate the 3D data.

which the procedure explained in the next section can be applied.

3. Wavelet representation

The wavelet transform is a multiscale tool that leads to a useful geometrical characterization of the signal $u(t)$ by allowing the detection and analysis of transient events. The wavelet transform is defined as [5,13]

$$U[\psi,u](b,a) = U_\psi(b,a) = \frac{1}{\sqrt{a}}\int_{-\infty}^{\infty} \psi^*\left(\frac{t-b}{a}\right)u(t)\,\mathrm{d}t, \tag{1}$$

$$U_\psi(b,a) = \sqrt{a}\int_{-\infty}^{\infty} \Psi^*(af)U(f)\mathrm{e}^{\mathrm{j}2\pi f\, b}\,\mathrm{d}f, \tag{2}$$

where $U_\psi(b,a)$ is the wavelet transform of $u(t)$, $a>0$ is the scale parameter and b is the shift parameter of the mother wavelet ψ. Eq. (2) represents the Fourier version of the wavelet transform. It should be noted that several mother wavelets may be used, depending on the type of information to be extracted from the signal [5,13]. The Morlet and the derivatives-of-Gaussian are among the most popular wavelets. In the Fig. 2(b), we see the application of the wavelet transform to a complex signal corresponding to a polygonal line. Fig. 2(c) shows a schematic representation of the wavelet transform by assigning each line of the wavelet coefficients matrix (that corresponds to the scale a value) (Fig. 2(b)) to a internal contour of the polygon (Fig. 2(a)). Note that the internal representation of the wavelet transform shows the relation of this transform to the curvature. This fact is highlighted by stronger responses at the landmarks $L1$, $L3$, $L5$, $L7$, $L9$ as indicated in Figs. 2(a)–(c). The more pronounced the curvature, the higher the related wavelet coefficient.

Differentiation operators from signal analysis have been widely applied to the characterization of shapes in applications such as classification of neural cells [5]. The next sections show how wavelets can be explored in order to extract meaningful differential shape descriptors.

3.1. Wavelet representation of 2D curves

In the 2D case, we follow the approach proposed in [13], in which the input to the wavelet transform is a complex signal representing the shape. Thus, the signal $u(t)$ can be defined as

$$u(t) = x(t) + jy(t). \tag{3}$$

As we see in [6], the convolution theorem [5,19] allows the application of the wavelet transform with the nth

derivative-of-Gaussian mother wavelet as an approximation of the nth derivative of $u(t)$. In the next section, we introduce a corresponding methodology for 3D data.

3.2. Wavelet representation of 3D curves

The adopted methodology for the extraction of wavelet coefficients from 3D data was to consider each dimension of a 3D signal $\vec{u}(t) = (x(t), y(t), z(t))$ as a 1D real-valued signal and to apply the wavelet transform to each of these. The 3D wavelet representation $\vec{U}(b,a)$ is formed from those coefficients, i.e.

$$\vec{U}(b,a) = (X(b,a), Y(b,a), Z(b,a)). \tag{4}$$

Referring to principles studied in [6], the wavelet transform with the nth derivative of Gaussian $g^{(n)}$ of $u(t)$ (denotaded as $U(b,a)$, with $\psi = g^{(n)}$) is an estimator of the nth derivative of $u(t)$. Then, for $\vec{u}(t) = (x(t), y(t), z(t))$ it is possible to calculate $X(b,a)$, $Y(b,a)$ and $Z(b,a)$ in order to estimate the nth derivatives of $x(t)$, $y(t)$ and $z(t)$, respectively. Thus, $X(b,a)$, $Y(b,a)$ and $Z(b,a)$ are related to the partial derivatives of $\vec{u}$ and the total derivative of $\vec{u}$ in t can then be estimated by the vectorial sum of these partial derivatives.

$$\vec{u}(t)^{(n)} \approx \vec{X}(b,a) + \vec{Y}(b,a) + \vec{Z}(b,a). \tag{5}$$

This implies that $|\vec{U}(b,a)|$ is an estimator of $|u^{(n)}|$. Therefore, $|\vec{U}(b,a)|$, with $\psi = g^{(1)}$ represents the length of the tangent vector of $\vec{u}$ in t and $|\vec{U}(b,a)|$, with $\psi = g^{(2)}$ is a measure of orientation variation, i.e. curvature, of $\vec{u}$. We have adopted the second derivative of Gaussian as the analyzing wavelet in the results reported in this paper. Thus, we can define the features used for the 2D and 3D samples.

Let L_i, $i = 1 \ldots N$, be the ith landmark, b_i be the shift parameter associated with L_i and A be the number of discretized scales. In this manner, we take as the 2D features

$$|U(b_i,a)|, \tag{6}$$

$$M_{scale}(a) = \frac{\sum_i |U(b_i,a)|}{N}, \tag{7}$$

$$V_{scale}(a) = \frac{\sum_i (|(U(b_i,a)| - M_{scale}(a))^2}{N-1}, \tag{8}$$

$$M_{land}(i) = \frac{\sum_a |U(b_i,a)|}{A}, \tag{9}$$

$$V_{land}(i) = \frac{\sum_a (|U(b_i,a)| - M_{land}(i))^2}{A-1}. \tag{10}$$

And for the 3D case, we use

$$|X(b_i,a)|, \tag{11}$$

$$|Y(b_i,a)|, \tag{12}$$

$$|Z(b_i,a)|, \tag{13}$$

$$|\vec{U}(b_i,a)|, \tag{14}$$

$$M_{scale}(a) = \frac{\sum_i |\vec{U}(b_i,a)|}{N}, \tag{15}$$

$$V_{scale}(a) = \frac{\sum_i (|\vec{U}(b_i,a)| - M_{scale}(a))^2}{N-1}, \tag{16}$$

$$M_{land}(i) = \frac{\sum_a |\vec{U}(b_i,a)|}{A}, \tag{17}$$

$$V_{land}(i) = \frac{\sum_a (|\vec{U}(b_i,a)| - M_{land}(i))^2}{A-1}. \tag{18}$$

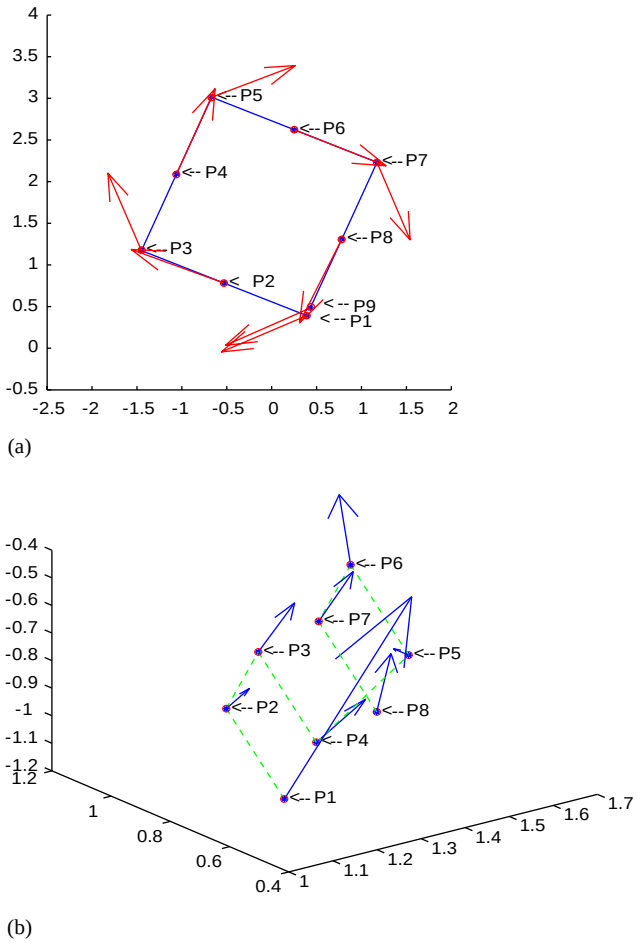

Fig. 4. (a) Estimative of the second derivative of the signal formed by $x(t)$ and $y(t)$ and (b) estimative of the second derivative of the signal formed by $x(t)$, $y(t)$ and $z(t)$.

4. Experimental results

4.1. Simulated data

In order to assess the performance of the introduced framework, simulated data sets with three and four different classes were created for the 2D (Fig. 3(a)) and 3D (Fig. 3(b)) cases, respectively. The procedure to obtain this data set was to add noise to a prototype model of each class (see examples in Fig. 3), generating 10 samples per class.

Fig. 4 presents the vectors obtained by the transform at the original landmarks (i.e. representing the corresponding second derivatives at each landmark).

Because of the wavelet redundancy across different scales of a selected feature an algorithm has been developed and applied to the wavelet features in order to select those that best categorize the classes in our application.

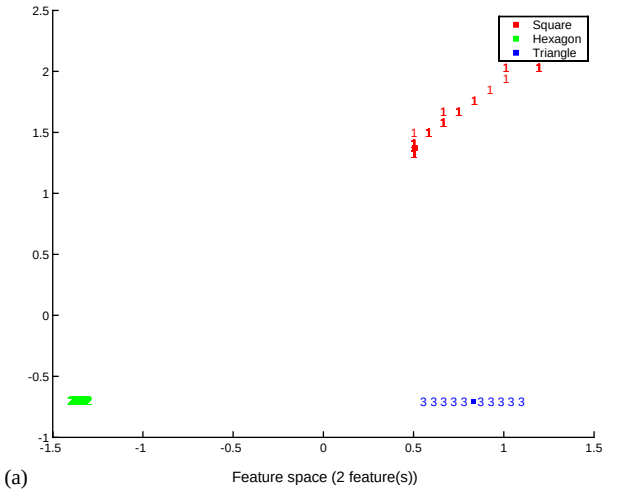

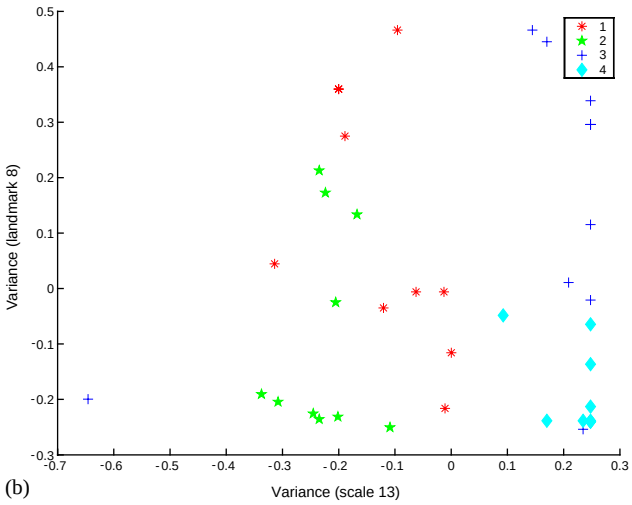

Fig. 5. (a) Feature space of the 2D simulated data (showing the $V_{land}(7)$ and $V_{land}(4)$) and (b) feature space of the 3D simulated data.

In order to speed the feature selection algorithm, only those features related to the landmarks positions were used. Thus, starting with the above-explained features, it is possible to identify which feature vectors provide a better classification. The applied procedure was used to test all 2×2 combinations of features by selecting training sets (randomly chosen $\frac{1}{3}$ of the input set) and testing (remaining $\frac{2}{3}$) with a minimum distance to prototype classifier [20]. The choice of the 2D feature spaces has been made to allow application of exhaustive methods, thus reducing the number of features and facilitating the extraction of biological interpretation in experiments with real data. Training and testing procedures were repeated for each feature set until convergence of the classifier error rate was reached.

The 2D and 3D data sets were classified and the resulting feature space using the best set of two features (i.e. variance of the wavelets coefficients at scale 13 and the variance at landmark 8) is shown in Fig. 5(a) and (b), respectively.

In the next sections, we present clustering results of real data related to two specific biological aspects: (a)

Table 1
Specimens of canids considered in our experiments

Code	Class	Specimens	Male	Female
1	*Atelocynus microtis*	13	7	6
2	*Cerdocyon thous*	24	12	12
3	*Chrysocyon branchiurus*	13	5	8
4	*Dusicyon australis*	2	1	1
5	*Lycalopex vetulus*	18	10	8
6	*Pseudalopex culpaeus*	30	15	15
7	*Pseudalopex gymnocercus*	30	15	15
8	*Pseudalopex sechurae*	10	5	5
9	*Speothos venaticus*	22	13	9
10	*Nyctereutes procyonoides*	11	5	6
Total		173	88	85

Fig. 6. Image of a skull of *Pseudalopex gymnocercus* showing landmarks digitized in dorsal view.

sexual dimorphism, an important source of intraspecific variability in biological species; (b) correlation between morphological or molecular descriptors and the evolutionary process, of major interest in morphometric analysis.

4.2. Morphology and sexual dimorphism

The previously presented methodology was also applied in order to analyze intraspecific variability in biological species by taking differences among males

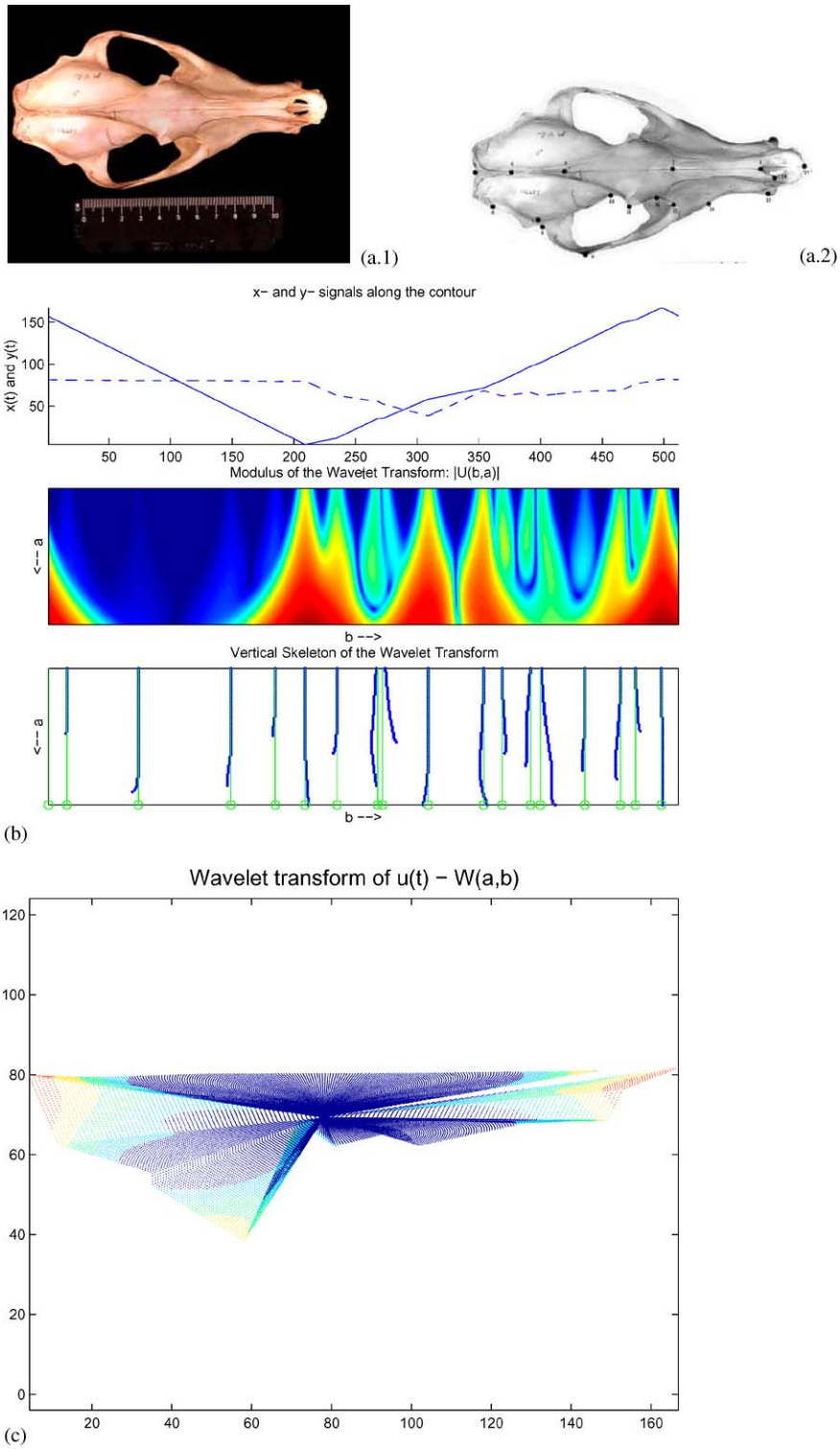

Fig. 7. (a.1) Dorsal view of one specimen of *A. microtis*; (a.2) landmarks taken from (a.1); (b) signal and wavelet-based representations of (a.1) and (c) internal wavelet representation of (a).

and females into consideration. Therefore, we took samples of all 10 species belonging to the South American Canids (Mammalia: Canidae) group (See Table 1). The goal was to study differences in size and shape among males and females, mapping the results of the two phylogenetic hypothesis already proposed for the canids, one molecular and the other constructed using morphological characters. Samples consisted of digital images of the dorsal surface of the skull of prepared specimens taken in various Natural History Museums, and including, when possible, the same number of adult males and females. We digitized 17 2D landmarks in each one of the 173 images (Fig. 6).

The wavelet features are used as input to an automated feature selection procedure that uses the Mahalanobis distances between male and female classes of all combinations of two features to select the set that best characterizes dimorphism. Thus, it is possible to

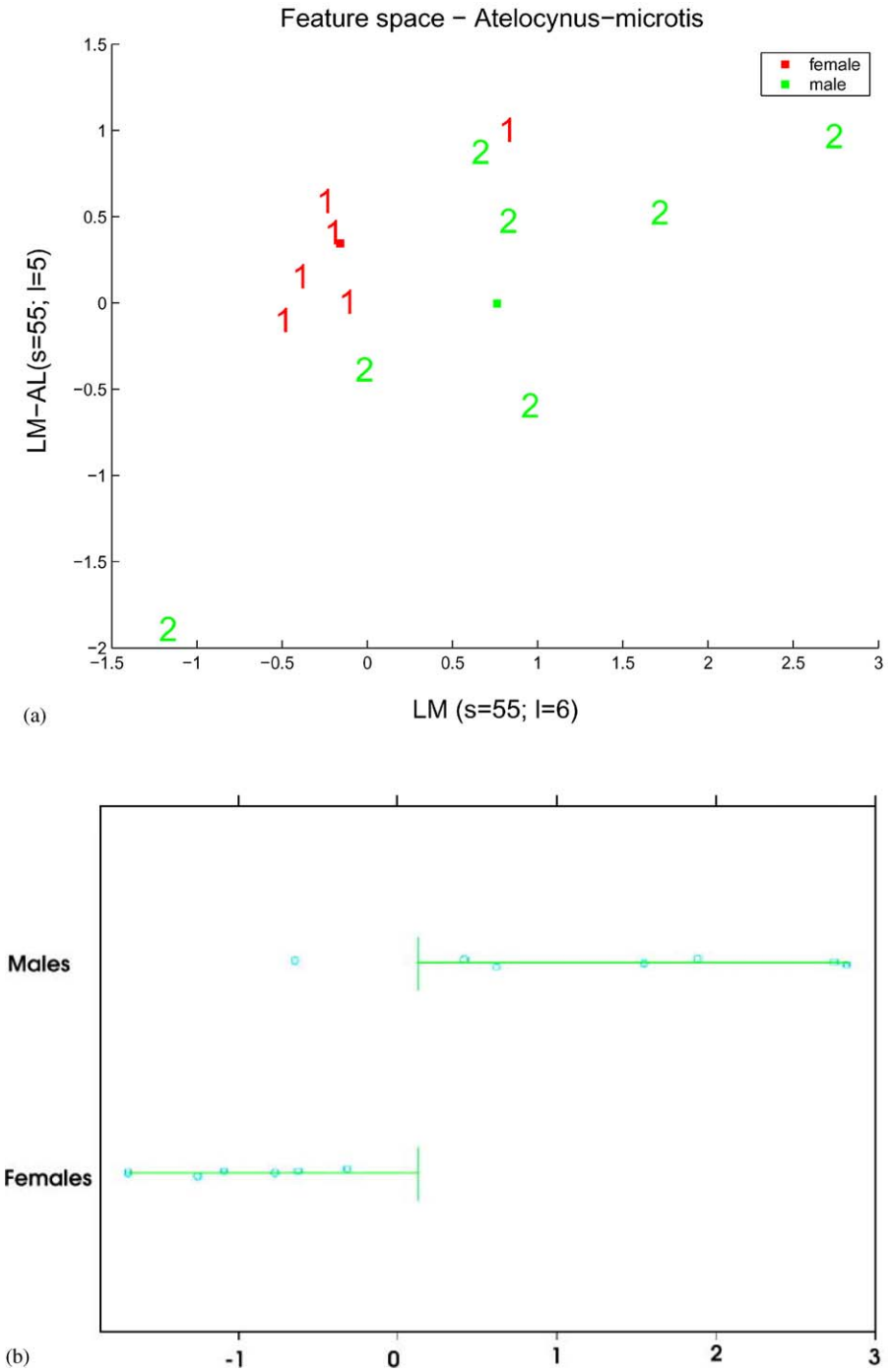

Fig. 8. (a) Feature space with two best discriminative features for *A. microtis* and (b) discriminate analysis of (a).

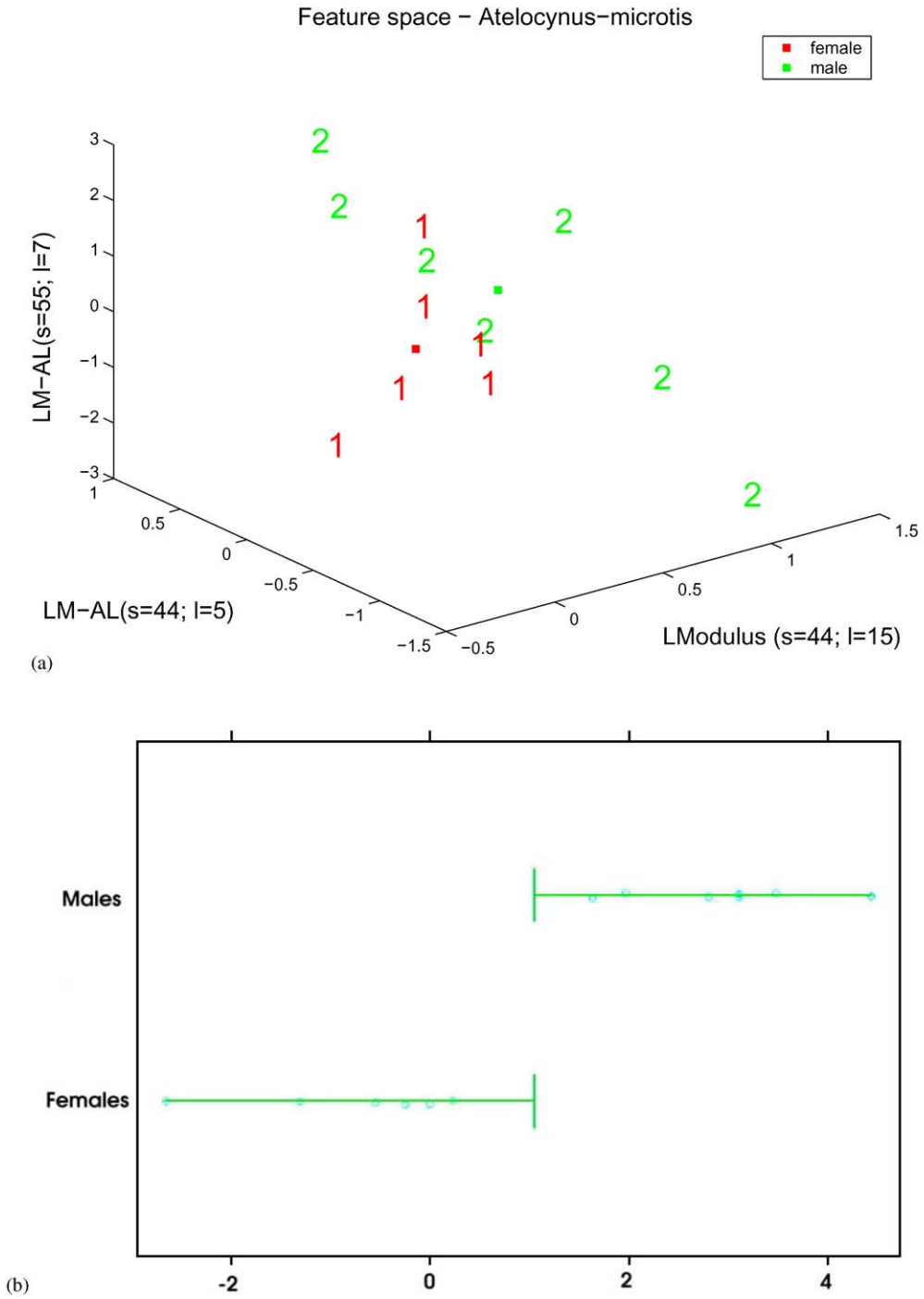

Fig. 9. (a) Feature space with three best discriminative features for *A. microtis* and (b) discriminate analysis of (a).

construct a rank of discrimination levels of the features then allowing a biological interpretation of the results. Fig. 7 shows the extraction of wavelet features using the landmarks from *Atelocynus microtis*. After selecting all the combinations of n features, the set that minimizes the distances between males and females, based on a canonical analysis of these features, is calculated for each class. Figs. 8(b) and 9(b) present a set of results using *A. microtis* as reference and sex as the independent variable (1 represents females specimens and 2 represents male).[1] Note, by using discriminant analysis we generated a better discrimination level for 3 features.[2]

[1]The best 2D feature space uses wavelets coefficients at landmarks 5 and 6 over the scale 55. The *AL* notation is used to identify wavelet coefficients that derive from signals aligned by Procustes normalization.

[2]The best 3D feature space are formed by wavelet coefficients at landmark 55 using scale 55; (b) at landmark 5 using scale 44; and (c) at landmark 15 using scale 44. The *Modulus* notation is used to identify the modulus of wavelet coefficients.

Table 2
Studied species

Code	Class	Specimens
1	*T. eliasi*	5
2	*T. paratus*	6
3	*T. s. denigratus*	9
4	*T. s. elegans*	5
5	*T. yonenagae*	16

The results demonstrate a separation between males and females in each class, but it was not possible to define a set of features that separates males and females in all classes at the same time. This is not surprising, since patterns of sexual dimorphism are expected to be different even among related species.

4.3. Morphology and phylogeny

In order to validate the use of 3D wavelet representation, we analyzed the relationship of morphological and phylogenetic patterns of the rodent genus *Trinomys* [21]. The studied specimens consisted of five taxa (*T.yonenagae*, *T.paratus*, *T.s.denigratus*, *T.s.elegans*, *T.eliasi*) of *Trinomys* (see Table 2), and each shape has 51 3D landmarks (Fig. 10).

These morphological landmarks were primarily defined on the basis of topological features of the cranium [22,23]. Each cranium was placed parallel to the focal plane under a Pixera (Pixera Corporation, Los Gatos, California) digital camera system and the *x*-, *y*- and *z*-coordinates of each landmark were obtained using PhotoModeler Lite software [24].

Using a total of 613 features ($X(b_i,a)$, $Y(b_i,a)$, $Z(b_i,a)$, $|\vec{U}(b_i,a)|$, $M_{scale}(a)$, $V_{scale}(a)$, $M_{land}(i)$, $V_{land}(i)$), the feature space in Fig. 11 was selected. In Fig. 11(b) it is possible to see the dendrogram of the distances between the mean values for each pair of classes.

The projection of specimens of the five species in the feature space defined by the variance of the wavelet coefficients at scale 63 and the wavelet coefficient at landmark 1 and scale 49 shows the distinctiveness of *T. yonenagae* relative to the other species. This result demonstrates that morphological descriptors of shape modeled by wavelets map onto patterns of ecological differentiation since *T. yonenagae* diverged uniquely in ecology and morphology from all others species *Trinomys* [25]. Contrary to species in this genus, which are ground dwellers in forest habitats, *T. yonenagae* inhabits fossil sand dunes in a restricted area in the left bank of the São Francisco river in the state of Bahia in north-eastern Brazil. The differentiation of *T. yonenagae* in this particular habitat has produced a strikingly distinct morphology involving a combination of traits such as a light-colored pelage, a well-developed tail brush, large hind feet and cranial modifications, including an inflated bulla [25]; all of which are usually associated with evolution in arid environments.

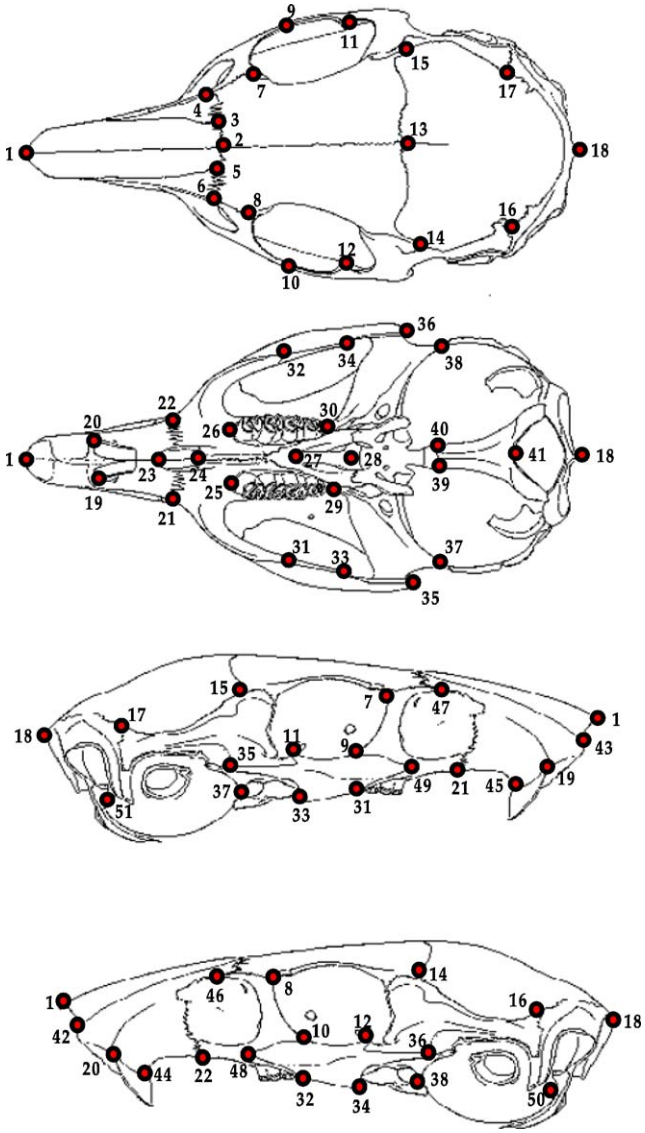

Fig. 10. Landmarks of *Trinomys*.

The uniqueness of ecological life-history and morphological traits of *T. yonenagae* are not paralleled by molecular differentiation as inferred from mitochondrial cytochrome *b* gene sequences, since *T. yonenagae* is well nested within a lineage which includes *T. elegans*, *T. paratus* and *T. eliasi*. Thus, there is a disparity between divergences at the organismal (ecological and morphological) and molecular (mitochondrial DNA sequences) levels.

It is evident that the wavelet representation mapped variation in cranial shape among the species of *Trinomys* onto the ecological component of differentiation that may have arisen from adaptation to distinct environments.

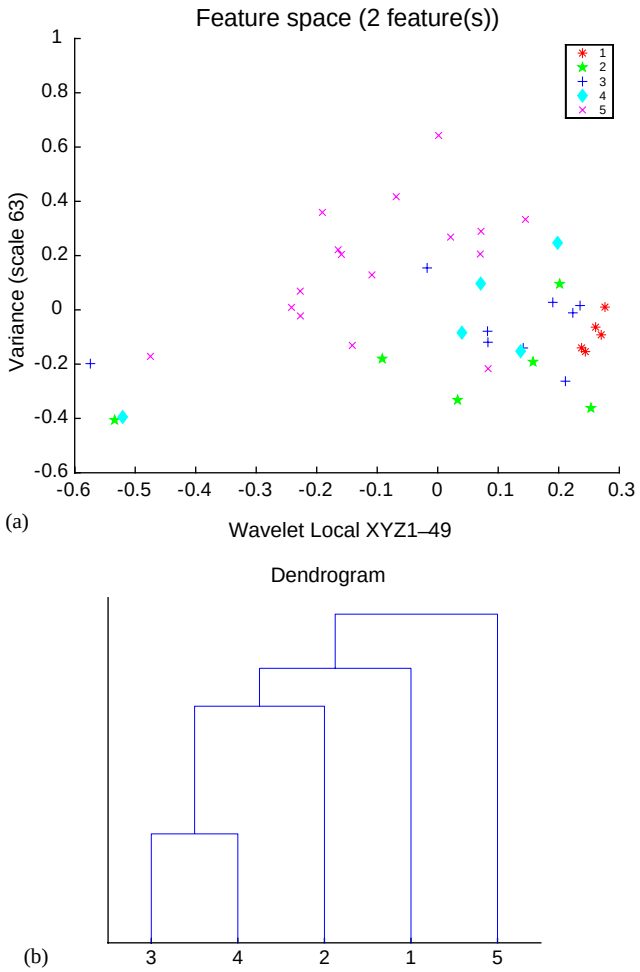

Fig. 11. (a) Feature space of the real data using the two features that best separate the species and (b) dendrogram of the distances of the mean value of each class.

5. Concluding remarks

In this paper, we show how it is possible to characterize biological shapes represented by 2D and 3D landmarks through multiscale and differential signal processing techniques in order to relate ecological and sexual variables with the morphology of a species. Results demonstrate that the wavelet transform can be used as a powerful descriptor of variation in shapes and can be successfully applied in morphometric studies. We claim that this is a generic technique that may be successfully applied to other types of 3D data, which belongs to our ongoing work besides further development of the current approach.

Acknowledgements

C.M. Takemura is grateful to CAPES for the financial support. R.M. Cesar-Jr. is grateful to FAPESP (99/12765-2) as well to as CNPq (300722/98-2).

The authors are grateful to Prof. Pete Lestrel for the suggestion of the contour-wavelet representation of Fig. 2.

References

[1] Bookstein FL. Morphometric tools for landmark data: geometry and biology. Cambridge: Cambridge University Press; 1992.
[2] Monteiro LR, dos Reis SF. Princípios de morfometria geométrica. Ribeirão Preto: Holos; 1999.
[3] Marcus LF, Traditional morphometrics. In: Rohlf FJ, Bookstein FL, editors. Proceedings of the Michigan morphometrics workshop: University of Michigan Museum of Zoology, 1990, p. 77–122 [Special Publication No. 2.].
[4] Martins EP. Adaptation and the comparative method. Tree 2000;15(7):296–9.
[5] Costa LF, Cesar- Jr RM. Shape analysis and classification: theory and practice. Boca Raton: CRC Press; 2001.
[6] Takemura CM, Cesar-Jr RM. Shape analysis and classification using landmarks: polygonal wavelet transform. In: Proceedings of the 15th European conference on artificial intelligence ECAI2002; 2002.
[7] Lestrel PE, Cesar- Jr RM, Takahashi O, Kanazawa E. A Fourier-wavelet representation of 2-d shapes: sexual dimorphism in the Japanese cranial base. Anthropological Science 2004;112(1):3–28.
[8] Rioul O, Vetterli M. Wavelets and signal processing. IEEE SP Magazine 1991; 14–38.
[9] Antoine JP. Wavelet analysis: a new tool in signal processing. Physicalia Magazine 1994;16:17–42.
[10] Arneodo A, Argoul F, Bacry E, Elezgaray J, Muzy J-F. Ondelettes, multifractales et turbulences: de l'ADN aux croissances cristallines. Paris: Diderot Editeur, Arts et Sciences; 1995 [in French].
[11] Castleman KR. Digital image processing. Wavelet transforms, Englewood Cliffs: Prentice-Hall; 1996. p. 303–47 [chapter 14].
[12] Grossmann A. Wavelet transforms and edge detection. In: Hazewinkel M, Albeverio S, Blanchard Ph, Streit L, editors. Stochastic processes in physics and engineering. Dordrecht: Reidel Publishing Company; 1988.
[13] Antoine JP, Barache D, Cesar-Jr RM, Costa LF. Shape characterization with the wavelet transform. Signal Processing 1997;62(3):265–90.
[14] Harvey PH, Pagel MD. The comparative method in evolutionary biology. Oxford: Oxford University Press; 1991.
[15] dos Reis SF, Monteiro LR, Monteiro-Filho ELA. Skull shape and size divergence in dolphins of the genus *Sotalia*: a tridimensional morphometric analysis. Journal of Mammalogy 2002;81(1):125–34.
[16] Monteiro LR, Diniz-Filho JAF, dos Reis SF, Araújo ED. Geometric estimates of heritability in biological shape. Evolution 2002;56(3):563–72.
[17] Bookstein FL, Chernoff B, Humphries J, Elder R, Smith G, Strauss R. Morphometrics in evolutionary biology. Academy of Natural Sciences of Philadelphia; 1985.
[18] Dryden IL, Mardia KV. Statistical shape analysis. Chichester: Wiley; 1998.
[19] Gonzalez RC, Woods RE. Digital image processing. Reading, MA: Addison-Wesley; 1992.
[20] Duda RO, Hart PE, Stork DG. Pattern classification. New York: Wiley; 2001.
[21] dos Reis SF, Duarte LC, Monteiro LR, Von Zuben FJ. Variation in mandible shape in *Thrichomys apereoides* (Mamalia: Rodentia): geometric analysis of a complex morphological structure. System Biology 2000;49(3):563–78.
[22] dos Reis SF, Duarte LC, Monteiro LR, Von Zuben FJ. Geographic variation in cranial morphology in *Thricomys*

apereoides (Rodentia: Echimyidae). I. Geometric descriptors and patterns of variation in shape. Journal of Mammalogy 2002; 83(2):333–44.

[23] dos Reis SF, Duarte LC, Monteiro LR, Von Zuben FJ. Geographic variation in cranial morphology in *Tricomys apereoides* (Rodentia: Echimyidae). II. Geographic units, morphological discontinuities, and sampling gaps. Journal of Mammalogy 2002;83(2):345–53.

[24] Flach S, Hargrave J, Moore S, Rempel G, Valji A, Walford N. Photomodeler lite (EOS Systems Inc.), 1999.

[25] Rocha PLB. *Proechimys yonenagae*, a new species of spiny rat (Rodentia: Echimyidae). Mammalia 1995;59:537–49.